Available online at www.sciencedirect.com
ScienceDirect
Polymer 47 (2006) 7318–7327
polymer
www.elsevier.com/locate/polymer

Bottle-brush macromolecules in solution: Comparison between results obtained from scattering experiments and computer simulations

Silke Rathgeber [a,*], Tadeusz Pakula [a], Agnieszka Wilk [a], Krzysztof Matyjaszewski [b], Hyung-il Lee [b], Kathryn L. Beers [c]

[a] *Max-Planck Institut für Polymerforschung, Polymerphysik, D-55128 Mainz, Germany*
[b] *Carnegie Mellon University, Department of Chemistry, Pittsburgh, PA 15213, USA*
[c] *National Institute of Standards and Technology, Polymer Division, Gaithersburg, MD 20899-8542, USA*

Received 9 March 2006; received in revised form 6 April 2006; accepted 12 April 2006
Available online 7 July 2006

Abstract

We addressed the structure of bottle-brush macromolecules under good solvent conditions by means of scattering techniques and computer simulations. Architectural parameters, such as backbone length, side chain length and side chain stiffness were varied systematically. A consistent description of the form factors was achieved by describing the bottle-brush polymers as flexible cylinders with internal density fluctuations. The model leads to direct conclusions about parameters, such as the brush persistence length, describing the overall shape of the bottle-brush polymers. Indirect conclusions about the side chain and backbone conformation can be drawn. Experimental results were compared to those obtained from computer simulations carried out for single bottle-brush polymers using the cooperative motion algorithm. The simulation gives direct access to the pair correlation function, allowing an independent determination of the form factor. In addition direct information about the side chain and backbone conformation can be obtained. The critical parameter for lyotropic behavior of bottle-brush polymer solutions is the ratio of brush persistence length to diameter which should be of order 10 or larger. Thus the discussion of the results is focused on the impact of the architectural parameters on the persistence of the bottle-brush polymers. Experimental results on the lyotropic behavior of a bottle-brush polymer are presented.

Keywords: Scattering techniques; Computer simulations; Bottle-brush polymers

1. Introduction

Bottle-brush polymers are highly-branched macromolecules where linear side chains are covalently bonded to a linear polymeric backbone in a dense manner [1]. Overcrowding of the side chains in the bottle-brush polymer leads to rather shape-persistent, stiff, cylindrical structures solely due to intra-molecular excluded volume interactions.

Despite the large number of experimental [2–9], simulation [10–18] and theoretical [12,19–23] studies dealing with the conformational properties of bottle-brush macromolecules in solutions, a number of questions still remain open. The crucial point is that the persistence of the overall bottle-brush macromolecule is significantly increased compared to the bare backbone. The backbone adopts a rather extended conformation in the brush compared to the corresponding free linear chain. However, there is no agreement on what the effect of increasing side chain length is, on both, the persistence length of the backbone as well as of the overall brush structure. Predictions vary from a strong increase of the persistence length (backbone [12], brush [7,20,22,23]) over a slight increase (backbone [4,8,12–14], brush [4,8,21]) to no impact (backbone [2,5,6,9,11], brush [2]) on the persistence length with increasing side chain length. Computer simulations reveal that the impact of the side chain length on the backbone persistence depends on side chain flexibility. Stiff side chains induce

* Corresponding author. Tel.: +49 6131 379 115; fax: +49 6131 379 100.
E-mail address: s.rathgeber@mpip-mainz.mpg.de (S. Rathgeber).

0032-3861/$ - see front matter © 2006 Published by Elsevier Ltd.
doi:10.1016/j.polymer.2006.06.010

a higher backbone persistence as well as a stronger increase of the persistence length with increasing side chain length than flexible side chains [15,16]. Another question still under discussion is, whether the conformation of the side chains is unaffected by steric congestion or if the conformation is significantly inflicted in space. Predictions vary from a side chain conformation undergoing an (almost) three-dimensional (3D) self-avoiding random walk (SAW) [2,6,9,11,12,17,21] to a conformation being closer to that of a two-dimensional (2D) SAW [7,10,13,18,20,22]. In the first case, the brush radius is expected to increase with the end-to-end distance of the side chains $\propto N_s^{3/5}$ whereas in the latter extreme case a $N_s^{3/4}$-dependence is expected. N_s denotes the number of segments constituting the side chains.

Concerning the possibility of lyotropic behavior of bottle-brushes in solutions, the critical parameter is the ratio of the persistence length, l_p, to the diameter, d, of the bottle-brush macromolecules. The driving force for ordering phenomena in bottle-brush polymer solutions are excluded volume interactions. In contrast to flexible cylinders with hard-core interactions, the bottle-brush macromolecules start to interpenetrate when the overlap concentration Φ^*, which can be rather low for brushes with long side chains, is exceeded. For concentration above Φ^* excluded volume interactions will gradually diminish, thus lyotropic behavior is expected to disappear again at somewhat higher polymer concentrations. As an estimate deduced from predictions for semi-flexible cylinders with hard-core interaction the ratio l_p/d should be of the order of 10 in order to lead to lyotropic behavior at reasonable concentrations [24].

We measured the full form factor of brushes synthesized by the ''grafting from'' route which consist of poly(*n*-butyl acrylate) (p*n*BA) side chains grafted from a poly(alkyl methacrylic) (pAMA) backbone. Experimental results are compared to results obtained from computer simulations. Conformational changes in the bottle-brush macromolecule are discussed under systematic variation of architectural parameters, such as backbone length, side chain length and side chain stiffness. Emphasis is placed on the impact of these structural parameters on the brush persistence and the ratio l_p/d. Experimental results of the lyotropic behavior of a bottle-brush polymer in concentrated solutions are shown.

2. Experimental

2.1. Samples

The architecture of the bottle-brush polymers was varied in a systematic manner. Parameters changed were the side chain length (series S) and backbone length (series B), keeping one of the parameters fixed. A schematic of the chemical structure of the investigated bottle-brush macromolecules is given in Ref. [2].

The samples consist of hydroxyethyl methacrylic main chains prepared by atom transfer radical polymerization [25,26]. As described in earlier publications [27,28], subsequent side chain functionalization with 2-(bromopropionyloxy)ethyl moiety yields initiation sites for controlled growth of P*n*BA side chains. The macroinitiators were prepared by polymerizing trimethylsilyl protected poly(2-hydroxyethyl methacrylate) [29,30].

Samples were characterized using size exclusion chromatography (SEC), ^{1}H nuclear magnetic resonance (NMR), elemental analysis (EA) and static light scattering. Sample characteristics, such as the weight and number averaged molecular weights, M_w and M_n, and the polydispersities M_w/M_n are summarized for most samples in Ref. [2]. The characteristics of the samples B-486-9 belonging to series S as well as the characteristics of the sample B-365-41 on which the lyotropic behavior was measured are summarized in Table 1. The characteristics of the corresponding macroinitiators are also included.

2.2. Scattering experiments

2.2.1. Static light scattering

The static light scattering (SLS) experiments were performed with a home built apparatus using a frequency doubled continuous wave Nd:yttrium–aluminum–garnet laser model DPY 425 II from Adlas, Germany with a wavelength of 532 nm and an avalanche diode model SPCM-PQ from EG&G, Canada as detector. The detected, scattered light was computed to correlation functions by a 50 000/E/ALV hardware correlator. Toluene was used as index matching bath. The temperature of the sample holder was kept constant

Table 1
Characteristics of the macroinitiators and bottle-brush polymers of the new samples

Macroinitiators					
Series	Name	Polymer	SEC		
			N_b (10^3 g/mol)	M_n (10^3 g/mol)	M_w/M_n (10^3 g/mol)
S	B-486-0	pBPEM	486	115.0	1.12
S	B-365-0	pBPEM	365	84.1	1.15

Bottle-brush polymers						
Series	Name	Macro-initiator	SLS		Model fit	
			N_s (10^5 g/mol)	M_w (10^5 g/mol)	N_s (10^5 g/mol)	M_w (10^5 g/mol)
S	B-486-9	B-486-0	9	6.85	10	7.54
S	B-365-41	B-365-0	41	20.1	44	21.5

The characteristics of all other samples are given in Ref. [2].

to 20 ± 0.1 °C. Static and dynamic light scattering data were collected simultaneously in 2° steps in a scattering angle range between 20° and 150° corresponding to a q range from 5.15×10^{-3} up to 3.4×10^{-2} nm^{-1}. The latter was calculated with the refractive index $n = 1.496$ of toluene.

Samples were prepared in toluene solutions and concentrations down to $\Phi_p = 3.5 \times 10^{-4}$ wt% were measured. Scattering spectra taken for the lowest polymer contents normalized to Φ_p overlap within experimental error indicating that the structure factor influence is negligible for the lowest concentration measured. Round quartz cuvettes purchased from Hellma, Germany, with a diameter of 20 mm were used as sample containers. The solvent contribution to the scattering was subtracted and the data were converted to absolute scattering intensities using toluene as standard. Specific refractive index increments $\partial n/\partial c$ were measured with a Schulz–Cantow-type differential refractometer.

2.2.2. Small-angle neutron scattering

The small-angle neutron scattering (SANS) experiments were carried out by the KWS2 instrument at the Dido reactor of the Forschungszentrum Jülich GmbH, Jülich, Germany. The neutron beam had an incident wavelength of $\lambda = 0.632$ nm and a band width of $\Delta\lambda/\lambda = 18\%$. With three detector distances set to $d = 2$ and 8 m using a collimation of $c = 8$ m and $d = 20$ m with $c = 20$ m, a q range between 2.5×10^{-2} and 1.7 nm^{-1} was covered. The temperature at the sample positions was kept constant at 20 °C using a circulating bath thermostat. Using standard procedures the measured spectra were corrected for detector sensitivity, converted to absolute intensities and corrected for background scattering from the solvent and empty cuvette. The instrumental resolution is considered in the fit routines following the procedure described by Pedersen et al. [31].

Rectangular Hellma quartz cuvettes with a path length of 2 mm were used as sample containers. Solutions were prepared in deuterated toluene with polymer concentrations Φ_p between 2 and 0.1 wt%. For polymer concentrations below $\Phi_p \leq 0.25$ wt% no structure factor influence could be detected (see static light scattering). To ensure a sufficient signal to background ratio the presented high-q data were taken at higher concentrations $\Phi_p \geq 1$ wt%.

2.2.3. Small-angle X-ray scattering

The small-angle X-ray scattering (SAXS) experiments were carried out with the High Brilliance Beamline ID2 at the European Synchrotron Radiation Facility (ESRF) in Grenoble, France. The incident beam had a wavelength of $\lambda = 0.1$ nm with a band width of $\Delta\lambda/\lambda = 0.02\%$. Using two detector distances the evaluated q range was 3×10^{-2} nm$^{-1} \leq q \leq 3.5$ nm^{-1}. Using standard procedures the measured intensities were converted to absolute intensities and corrected for background scattering and detector sensitivity. Experimental resolution effects, even so small were considered in the fit routines. As sample containers sealed aluminum containers with mica windows and a path length of 1 mm were used. In analogy to the neutron scattering experiments solutions were prepared in toluene with polymer concentrations Φ_p between 5 and 0.1 wt%.

2.2.4. Data modeling

We interpreted our scattering spectra by describing the overall shape of the bottle-brush polymers by a worm-like cylinder with a radial density profile. A detailed description of the model and the fitting procedure has been given in an earlier publication [2]. Here we would like to focus on the most important equations necessary for the interpretation of the results.

In case the Kuhn length of the cylinder is much larger than the cross section of the cylinder, the form factor of a worm-like cylinder $P_{shape}(q)$ can be decomposed into the product of the form factors of an infinite thin, semi-flexible chain $P_{wlc}(q)$ and the cross section form factor $P_{CS}(q)$

$$P(q) = P_{wlc}(q) \times P_{CS}(q) \tag{1}$$

where q is the norm of the scattering vector.

For the form factor of a semi-flexible chain $P_{wlc}(q)$ under good solvent conditions we used the empirical equations derived by Pedersen and Schurtenberger in Ref. [32] (method 3 under good solvent conditions). The adjustable parameters in the equations for $P_{wlc}(q)$ are the brush contour length L, the brush persistence length l_p and the Flory exponent ν which is related to the fractal dimension D of the overall brush by $D = 1/\nu$.

The cross section form factor $P_{CS}(q)$ is obtained by two-dimensional Fourier transform of the radial excess scattering length density profile $\rho_{CS}(r)$

$$P_{CS}(q) = \left| C^{-1} \int_0^\infty \rho_{CS}(r) J_0(qr) r \, dr \right|^2 \tag{2}$$

with $C = \int_0^\infty \rho_{CS}(r) r \, dr$. J_0 denotes the zeroth-order Bessel function of first kind and r is the radial distance from the cylinder axis perpendicular from the contour line. For $\rho_{CS}(r)$ we considered two scenarios. The first approach describes $\rho_{CS}(r)$ by an exponentially decaying cross section profile where the density is constant inside a dense core region but shows a generalized power-law decay in a more or less extended shell region (see Eq. (3) in Ref. [2]). For an exponent $x \approx 0$ a constant profile is modeled, while for $x = 4/3$ a star-like profile is obtained. The cross section form factor has to be calculated numerically. The second approach describes the radial density profile by a convolution of that of a homogeneous sphere with radius R_C and a Gaussian density profile with standard deviation σ_C. Depending on the ratio σ_C/R_C, a density profile with a more or less extended dense core region and a smoothly decaying density in a smeared shell region is obtained. R_C gives the radius of the analogous, homogeneous sphere and σ_C is a measure of the width of the surface region. For this profile an analytical expression for the cross section form factor can be derived (see Eq. (5) in Ref. [2]).

The cross section radius of gyration $R_{CS,g}$ can be calculated from the cross section density profile by

$$R^2_{CS,g} = \frac{\int_0^\infty r^3 \rho_{CS}(r) dr}{\int_0^\infty r \rho_{CS}(r) dr} \quad (3)$$

from which in case of the density profile described in the second approach an analytical expression can be obtained

$$R^2_{CS,g} = \frac{R^2_C}{2} + 4\sigma^2_C \quad (4)$$

On small length scales or large q values internal density fluctuations arising from the loose polymeric substructure of the bottle-brush polymers significantly contribute to the scattering. On length scales smaller than the correlation length of the density fluctuations ξ, parts of the bottle-brush polymers have to be described as self-avoiding random walks under excluded volume interactions with a fractality $D_f = 1/\nu_f$, where ν_f is the corresponding Flory exponent. We adopted the approach of Dozier et al. [33], in which the overall form factor of the bottle-brush polymer can be approximated by the sum of two contributions

$$P(q) = P_{shape}(q) + P_{fluc}(q) \quad (5)$$

The scattering contribution $P_{shape}(q)$ stemming from the overall shape is defined by Eqs. (1)–(3) and Eq. (5) given in Ref. [2].

The second term

$$P_{fluc}(q) = a_f \frac{\sin[\mu \tan^{-1}(q^*_f)]}{\mu q^*_f [1 + q^{*2}_f]^{\mu/2}} \quad (6)$$

with

$$q^*_f = \frac{q\xi}{\left[\mathrm{erf}(qR_{CS,g}/\sqrt{6})\right]^3} \quad (7)$$

and $\mu = \nu_f^{-1} - 1$, describes the contribution of the density fluctuations with a_f being the amplitude of $P_{fluc}(q)$ relative to $P_{shape}(q)$. The error function in Eq. (7) ensures a smooth vanishing of the scattering contributions stemming from the internal density fluctuations on length scales of the cross section radius of gyration. $P_{fluc}(q)$ adds the correlation length of the density fluctuations ξ and the fractality of the local structure $D_f = 1/\nu_f$ as adjustable parameters.

Finally, we took into account the polydispersity of the macroinitiators by assuming a Schulz–Zimm distribution for the contour lengths L. The polydispersity of the side chains was not explicitly considered in the fit but rather was included in the radial density profile. The radial density profiles of all brushes with side chain length $N_s \geq 41$ are well described by simple Gaussians

$$\rho_{CS}(r) = \exp\left(-\frac{r^2}{4\sigma^2_C}\right) \quad (8)$$

Only the density profiles of the samples with the shortest side chains $N_s = 9$ and 22 are better described by an exponentially decaying cross section profile as given in Eq. (3) of Ref. [2]. In Table 2 all fit parameters obtained for all samples relevant for the following discussion are summarized. Ref. [2] gives a detailed description of the fitting procedure and summarizes the fit parameters not given in Table 2.

2.3. Computer simulation

Monte-Carlo simulations of single bottle-brush macromolecules were carried out using the cooperative motion algorithm (CMA). Since conformational rearrangements are performed by cooperative motions of connected lattice beads, this method has been proven to be in particular suitable for the simulation of dense macromolecular systems where all lattice sites are occupied. In highly-branched polymer architectures such as dendrimers, high-functionality star polymers and bottle-brush macromolecules the internal segment densities can become comparable to those in bulk systems. We applied the CMA in a version previously applied to the simulation of single macromolecules with various architectures. For a detailed description of the method we refer to former publications [34,35]. Here we will focus only on those details relevant for the simulation of the bottle-brush polymers.

Single bottle-brush polymers, considered here under athermal conditions (good solvent) are constructed on a fcc

Table 2
Summary of the structural parameters and results obtained for the bottle-brush polymers from the model fit of the scattering spectra described in the text, including one macroinitiator M2 and the side chains corresponding to linear polymer S1

Series	Name		N_b	N_s	$R_{CS,g}$ (nm)	l_p (nm)	$l_p/(2R_{CS,g})$	L (nm)	L/l_p
	Old	New							
	S1	B-0-281	0	281	0.41 ± 0.02	0.47 ± 0.04	0.57 ± 0.05	71 ± 2	151 ± 14
	M2	B-400-0	400	0	0.99 ± 0.08	0.9 ± 0.1	0.45 ± 0.05	101 ± 3	112 ± 13
S	B1	B-486-9	486	9	2.61 ± 0.04	27 ± 3	5.2 ± 0.6	106 ± 4	3.9 ± 0.5
S		B-400-22	400	22	4.16 ± 0.08	35 ± 2	4.2 ± 0.3	112 ± 4	3.2 ± 0.2
S		B-365-41	365	41	5.12 ± 0.09	35 ± 2	3.4 ± 0.2	113 ± 4	3.2 ± 0.2
S/B	B2	B-400-62	400	62	6.3 ± 0.1	35 ± 2	2.8 ± 0.2	133 ± 4	3.8 ± 0.2
S	B3	B-400-98	400	98	8.2 ± 0.2	35 ± 2	2.2 ± 0.1	151 ± 5	4.3 ± 0.3
B	B4	B-188-58	188	58	6.0 ± 0.1	35 ± 2	2.9 ± 0.2	77 ± 2	2.2 ± 0.1
B	B5	B-780-50	780	50	5.8 ± 0.1	35 ± 2	3.0 ± 0.2	223 ± 7	6.4 ± 0.4

Old names, as given in Ref. [2] are included.

Table 3
Summary of the structural parameters of the simulated bottle-brush polymers: backbone length N_b, side chain length N_s and side chain stiffness in terms of the number of monomers N_c attached to each side chain monomer

N_s		0	1			2			5			10			20			50		
N_c			0	1	2	0	1	2	0	1	2	0	1	2	0	1	2	0	1	2
N_b	10	X	X			X			X			X			X			X		
	20	X	X			X	X	X	X	X	X	X	X	X	X	X	X	X	X	X
	50	X	X			X	X	X	X	X	X	X	X	X	X	X	X	X	X	X
	100	X	X			X			X			X	X	X	X					
	200	X	X			X			X			X			X					
	400	X	X																	

lattice without external boundaries. The bottle-brush skeleton is built by assemblies of beads connected by non-breakable bonds. Sizes and distances are expressed in unit a corresponding to the length of half of the fcc lattice constant, thus the bond length is $a\sqrt{2}$. In analogy to the real synthetic ''grafting from'' route the bottle-brush macromolecules were constructed according to the assumed structural parameters from a linear backbone from which linear side chains are grown by successively adding monomers (beads). During the growth process the structure was kept in motion resulting in almost spatially relaxed structures immediately.

In the simulated architectures, the backbone length N_b and side chain length N_s were varied, while the grafting density was kept fixed to 1; thus every bead carries one side chain. Variation of the side chain stiffness was achieved by adding side chains which are themselves bottle-brush polymers with one or two beads ($N_c = 0, 1, 2$) connected to each monomer, forming a double brush structure [36]. Table 3 summarizes the structural parameters of the simulated bottle-brush polymers.

A large number of conformations, as shown in the snapshot presented in Fig. 1 were generated by continuous cooperative movements of beads. To ensure that equilibrium is reached, dynamic correlation functions describing orientational and translational relaxation were monitored over time intervals exceeding the longest relaxation by at least one order of magnitude. The following quantities describing the conformation and dimensions of bottle-brush polymers were determined as averages taken over conformational snapshots considered to belong to equilibrium states:

(1) Center-of-mass coordinate

$$r_{cm} = \frac{1}{N}\sum_{i=1}^{N} r_i \tag{9}$$

Fig. 1. Snap-shot of a simulated bottle-brush polymer.

where r_i is the space coordinate of the ith bead and N is the total number of beads constituting the bottle-brush polymer.

(2) Mean square radius of gyration

$$\langle R_g^2 \rangle = \frac{1}{N}\sum_{i=1}^{N} \left\langle (r_i - r_{cm})^2 \right\rangle \tag{10}$$

(3) Mean square end-to-end distance

$$\langle R_E^2 \rangle = \left\langle (r_N - r_1)^2 \right\rangle \tag{11}$$

(4) Site–site correlation function of sites separated by $r_{ij} = r_i - r_j$

$$\gamma(r_{ij}) = \frac{1}{N}\langle c(r_i)c(r_j)\rangle \tag{12}$$

where c is a contrast operator assuming values of 1 for sites occupied by beads and 0 elsewhere.

(5) Static form factor

$$P(q) = \sum_{j=1}^{N}\sum_{i=1}^{N} \gamma(r_{ij}) \frac{\sin(qr_{ij})}{qr_{ij}} \tag{13}$$

(6) Bond–bond correlation function

$$C_{bb}(n) = \langle \alpha(i)\alpha(i+n)\rangle \tag{14}$$

defined as the average over all pairs of bond vectors α separated by n other bonds. $C_{bb}(n)$ is normalized so that $C_{bb}(0) = 1$.

(7) and as a measure of the chain persistence, we define the quantity

$$l_p^* = \sum_{n=0}^{N} C_{bb}(n) \tag{15}$$

We want to point out that l_p^* is not the persistence length and stays always smaller or equal to the number of segments constituting the chain.

Similar quantities can be defined for the terminal units, side chains and backbone, when the indices number monomers belonging to the selected parts of the bottle-brush polymers.

3. Results and discussion

The aim of the simulation was to conduct allow a systematic investigation on which impact architectural parameters such as side chain length N_s, backbone length N_b as well as side chain stiffness (N_c) have on the structural properties of the bottle-brush polymers. The scattering experiments were carefully designed in a systematic manner to enable us to investigate if the results obtained by computer simulation find experimental support. A comparison between the simulation data and the experimental data serves as basis to establish reference points which facilitate the following discussion.

We introduce the following nomenclature for the brushes: B-"N_b"-"N_s"-"N_c", where N_c is given for the simulated brushes only. Fig. 2 shows a comparison between the scattering spectra obtained for a representative bottle-brush polymer including its bare backbone (macroinitiator) and the form factors calculated using Eq. (13) from the simulated structures. To allow a comparison between experimental and simulated spectra the calculated form factors were convoluted with the experimental resolution. The experimental form factor of the bare backbone B-400-0 itself is best compared with the form factor of a simulated bottle-brush polymer B-100-1-0. The real bottle-brush polymer B-400-62 corresponds best to the simulated bottle-brush B-100-20-2. Scaling factors for the axes of the simulated spectra were obtained by taking the bare backbones B-400-0 (real system) and B-100-1-0 (simulated system) as reference. The x-axes were rescaled by comparing the radius of gyration of the simulated backbone determined using Eq. (10) with that obtained for the real backbone by a Guinier evaluation of the scattering spectrum. The y-axes are rescaled to give best agreement between the simulated and the experimental spectra of the bare backbone.

As a consequence of the intrinsic persistence of the polymers building the backbone and the side chain of the real system, a better description of the experimental data is achieved when an additional stiffness is induced in the simulated polymers. The real backbone is better characterized by a brush polymer itself with one side chain monomer. The side chains of the real bottle-brush polymers are even less flexible requiring two additional side chain monomers in the side chains themselves. This behavior finds support in the scattering experiments. As summarized in Table 2, the side chain polymer B-0-281 has a higher persistence than the backbone polymer B-400-0, which is consistent with $N_s = 1$ for the simulated backbone and $N_c = 2$ for the side chains in the brush.

The form factors of brushes with different backbone length ($N_b = 188, 400, 780$) but essentially constant side chain length ($N_s = 56 \pm 6$) as well as of brushes with equal backbone length ($N_b \approx 400$) but varying side chain length ($N_s = 9, 22, 41, 62, 98$) were measured by scattering techniques. The two sets of samples are referred to as series B and S, respectively. Series S includes also the bare backbone B-400-0. In Figs. 3 and 4 the experimental spectra normalized to the polymer concentration obtained for samples belonging to series S and B by means of SLS and SANS experiments are compared to those calculated from the simulation results. Here the y-axes are compared by plotting the same number of decades for the simulated and the experimental spectra. Since the scattering spectra obtained for the brushes B-365-41 and B-486-9 were measured with a much higher experimental resolution using SAXS the results are not included in Fig. 4. The scattering spectra for the samples of series B shown in Fig. 3 superimpose in the intermediate and high-q region where the

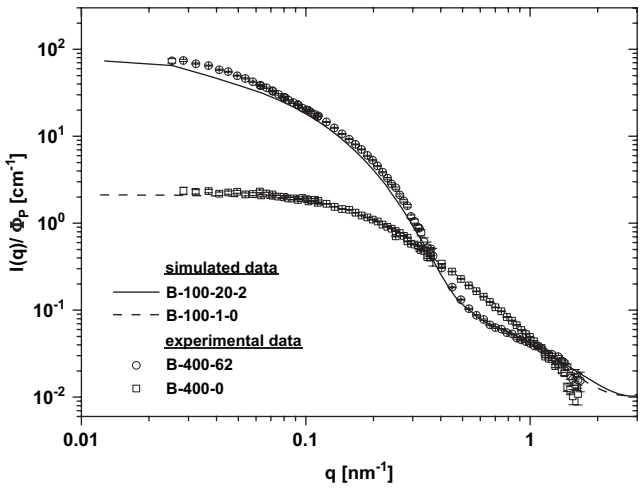

Fig. 2. Adjustment of experimental (markers) and simulated (lines) scattering spectra for brushes with varying grafting density.

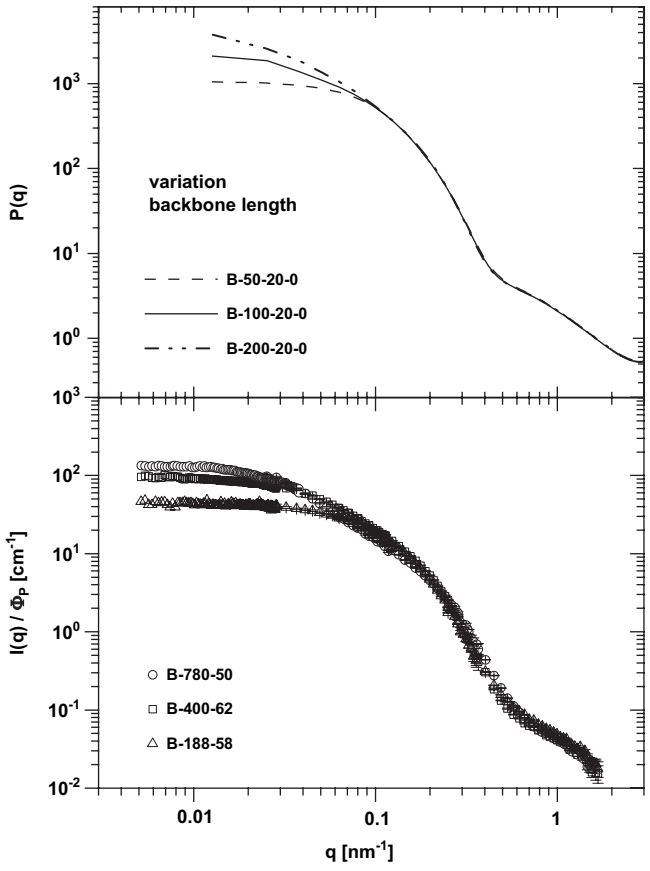

Fig. 3. Variation of backbone length: experimental scattering spectra and simulated spectra are shown in the bottom and top parts, respectively.

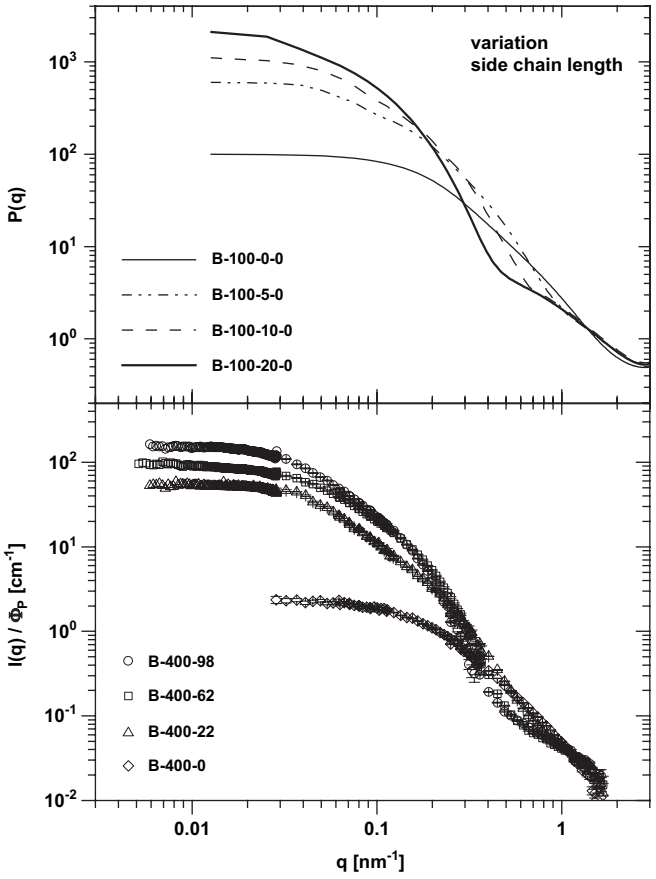

Fig. 4. Variation of side chain length: experimental scattering spectra and simulated spectra are shown in the bottom and top parts, respectively.

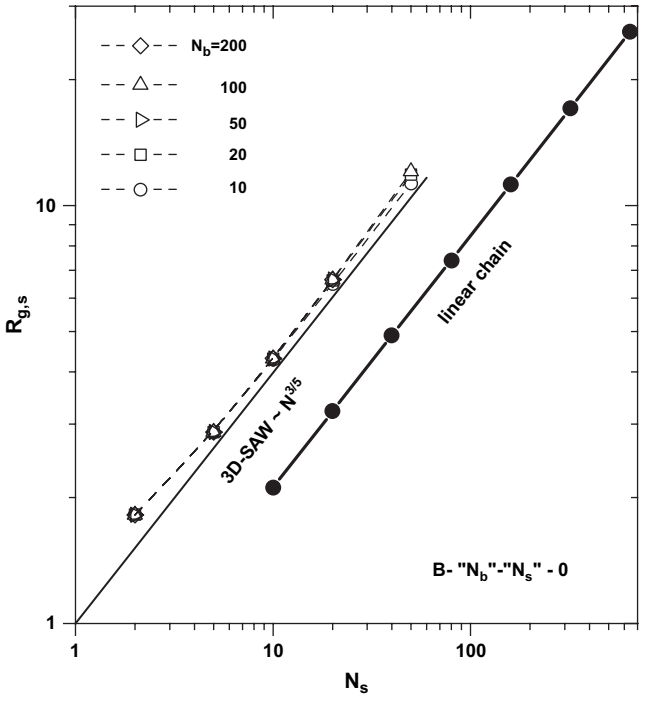

Fig. 5. Side chain radius of gyration as a function of side chain length (markers) in a double-logarithmic presentation for brushes with various backbone lengths. Dashed lines are just guides to the eye. The thin, solid line shows the dependency expected for a 3D-SAW. The thick solid line shows the results for the radii of gyration of simulated free, linear polymers of various length.

scattering is sensitive to the internal density fluctuations and the radial density profile, respectively. These observations indicate that the fractality of the side chains close to the periphery of the brush and the radial density profiles are equal for samples with different backbone length but constant side chain length. The scattering spectra split in the low-q region due to the different molecular weights of the samples. In Fig. 4 the spectra for samples belonging to series S are shown. Spectra still superimpose in the high-q region but split in the intermediate-q region as a consequence of significant changes in the density profiles due to the different side chain length. All these features are very well reproduced in the computer simulation results. We obtain good qualitative agreement between the experimental and simulated spectra.

Fig. 5 shows the impact of side chain and backbone length variation on the radius of gyration of the side chains $R_{g,s}$ of the simulated structures. The power-law dependence of the side chain radius of gyration on the side chain length $R_{g,s} \propto N_s^{\nu}$ approaches that of a 3D-SAW for the longer side chains ($\nu = 0.60$). The scaling behavior of the cross section radii of gyration $R_{CS,g}$ determined for the real bottle-brushes from the scattering experiments can be taken as a measure of the side chain fractality. As discussed in Ref. [2] a similar exponent $\nu = 0.57 \pm 0.03$ has been found. In Fig. 5 the radii of gyration of simulated free linear chains are also included. Obviously, the absolute values for $R_{g,s}$ of the side chains in the brush are increased compared to a free linear chain by a factor of 2. Similar findings where obtained from the experimental results where a factor of about 3 between $R_{CS,g}$ and that estimated from the free, linear chain dimension were obtained [2]. Thus, both experiment and simulation indicate a 3D-SAW for the side chain conformation. However, the step length of the SAW or equivalently the persistence length is larger than that of the corresponding free, linear chain.

As a measure of the backbone stretching, the relative change of the end-to-end distance of the backbone in the brush $R_{E,b}(N_s)$ compared to the end-to-end distance of the bare backbone $R_{E,b}(N_s = 0)$ is considered:

$$\mathrm{RS} = \left(\frac{R_{E,b}^2(N_s) - R_{E,b}^2(N_s = 0)}{R_{E,b}^2(N_s = 0)} \right)^{1/2} \tag{16}$$

In Fig. 6, the relative stretching RS is plotted as a function of side chain length for brushes with various backbone length. Increasing the side chain length causes an extension of the backbone. For long side chains, longer than about $N_s \approx N_b/2$ a saturation effect is observed. The saturation is not due to full stretching of the main chain. The ratio of $R_{E,b}(N_s)$ to the value of $R_{E,b}$ expected in case the backbone adopts a fully stretched conformation, stays below 0.5 for all simulated brushes.

The absolute values of the backbone stretching as well as the initial slope of RS with N_s increase with increasing side chain length and backbone length. No power-law dependency

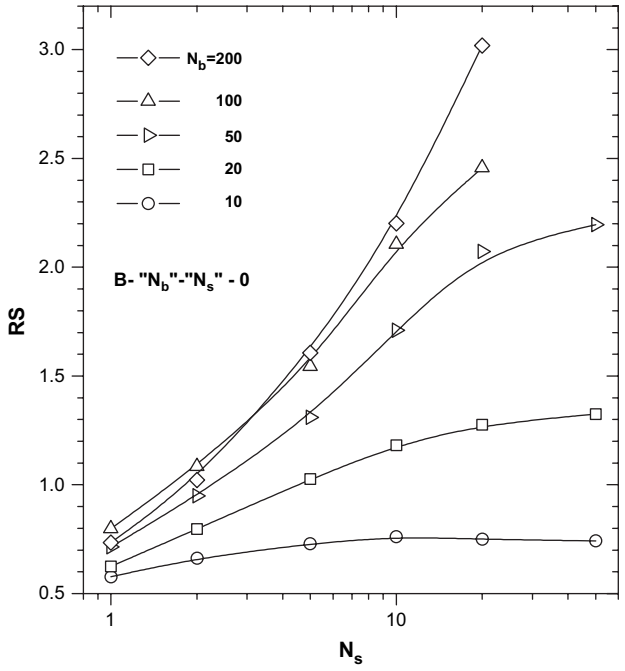

Fig. 6. Stretching of the backbone relative to the bare backbone as a function of side chain length for brushes with various backbone lengths. Lines are just guides to the eye.

of the end-to-end distance of the backbone on the backbone length was found for any side chain length (not presented) since l_p^* as a measure of the main chain persistence changes as a function of N_s and N_b as shown in Fig. 7. The persistence of the backbone shows the same dependency on the side chain and backbone length as the end-to-end distance of the backbone. Side chain stiffness is induced in the simulated structure by increasing N_c from 0 to 2. As plotted in the bottom part of Fig. 7 increasing the side chain stiffness leads to higher values for the backbone persistence and an increasing initial slope for the dependency of l_p^* on N_s for short side chains. Values of l_p^* range from about $l_p^* = 2 - 3.4$ for B-"N_b"-1-0 up to $l_p^* = 28$ for B-50-50-2. The persistence of the bare backbones was determined to be $l_p^* = 1.6$.

In conclusion, side chains, and consequently grafting points on the backbone repel each other due to excluded volume interactions. For longer side chains, the backbone stretches to allow the side chains to attain the entropically more favorable, coiled conformation. The loss in entropy due to stretching of the backbone is overcompensated by the conformational gain in entropy in the large number (N_b) of side chains. The saturation effect seen for longer side chains might indicate that inner side chain segments interfere more strongly with each other but outer segments find enough space to arrange almost freely in three dimensions. The increase in l_p^* with increasing backbone but fixed side chain length might originate from finite chain length effects due to the higher flexibility of the backbone close to the chain ends (end-caps of the cylindrical bottle-brush polymer). Bigger volume is available for the side chains at the cylinder ends, thus, extension of the backbone has no significant relevance for the conformational entropy of the side chains.

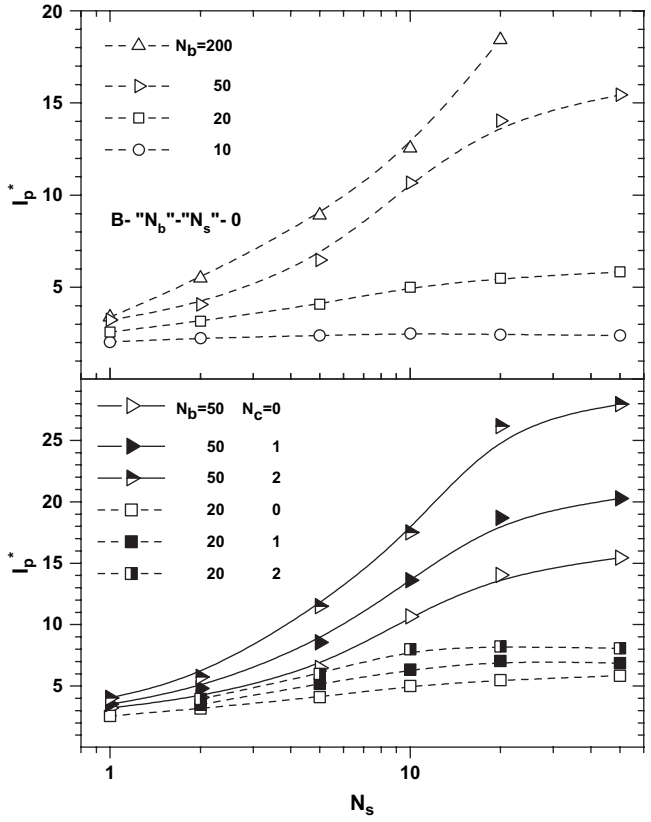

Fig. 7. l_p^* as a measure of the backbone persistence as a function of side chain length: (top) for various backbone length and (bottom) for two selected backbone length as a function of side chain stiffness. Lines are just guides to the eye.

The scattering experiment gives only indirect information about the backbone conformation in terms of the contour length per monomer contributing to the length of the flexible cylinder $l_b = L/(N_b + 2N_s)$ which was determined to be $l_b = 0.253 \pm 0.008$ nm for both, the brushes with $N_s \geq 22$ as well as for the bare backbone [2]. An identical l_b for the cylindrical bottle-brush polymer and the bare backbone should only be possible if the contour length of the flexible cylinder used to describe the bottle-brush follows that of the bare backbone. However, this should only be possible if the backbone in the brush attains a rather stretched conformation. For the brush B-486-9 with the shortest side chains $l_b = 0.21 \pm 0.01$ nm turns out to be slightly smaller. For the real bottle-brush polymers we obtained for the persistence length of the overall macromolecule $l_p = 35 \pm 2$ nm, independent of the side chain and backbone length for samples with $N_s \geq 22$. Only the sample B-486-9 with the shortest side chains exhibits a lower persistence length of about $l_P = 27 \pm 3$ nm. As discussed above, the representative brush B-400-62 is best described by a simulated brush B-100-20-2. Even though the persistence length of the backbones in the simulated brushes changes more strongly, we should have in mind that the changes with N_s and N_b in the end-to-end distance for the simulated brushes are not as drastic (±25%) for longer side chains, the error in the experimental determination of the persistence length is of the order of ±10% and the experiment measures the persistence length of the overall brush rather than that of the backbone as

the simulation does. The observed differences are most likely within the error bars of the experiment. Since the persistence length of the overall brush is (almost) constant, the ratio of persistence length to brush diameter d decreases with increasing side chain length and lyotropic behavior becomes more and more unlikely. For our particular system l_p/d decreases from 4 to 2 by increasing the side chain length from about $N_s = 22$ to 98. Here, the diameter d was assigned to $d = 2 \times R_{CS,g}$. Since the persistence length starts to decrease for bottle-brush polymers with shorter side chains ($N_s = 9$), decreasing N_s further does not lead to much higher ratios $(l_p/d \approx 5)$.

An important result of our investigations on the influence of architectural parameters on the conformation of bottle-brush polymers is that the ratio l_p/d can only be influenced to a slight extent by variations in the side chain and backbone length. However, l_p/d has to be large enough to obtain lyotropic phase transitions before interpenetration of the brushes leads to screening of the excluded volume interactions at elevated polymer concentrations. In the following section we study the lyotropic behavior of the bottle-brush polymer B-365-41.

In Fig. 8 scattering spectra are shown obtained for various polymer concentrations ranging from $\Phi_P = 4.0$ vol% up to 34.7 vol%. The length scale probed by the scattering experiment is of the order of the cylinder cross section. Starting from a polymer content of 16.6 vol%, higher order peaks appear which shift towards higher q values with increasing polymer concentration. Up to three orders of Bragg peaks can be resolved of which the positions are in the ratio $q_0 \div q_1 \div q_2 \div q_3 = 1 \div \sqrt{3} \div 2 \div \sqrt{7}$ as expected for hexagonal arrangements of aligned cylinders. This ratio is marked in Fig. 8 by the dashed vertical lines for the sample with $\Phi_P = 16.6$ vol%. The position of the first peak q_0 is related to the distance between the centers of adjacent cylinders d_c by

$$d_c = \frac{2}{\sqrt{3}} \frac{2\pi}{q_0} \tag{17}$$

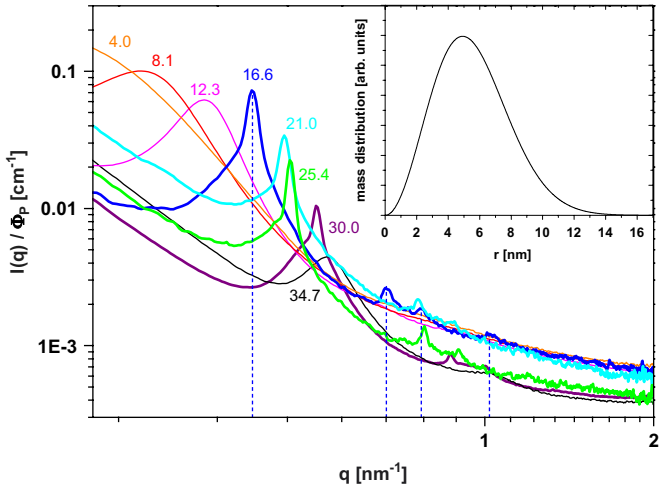

Fig. 8. Scattering spectra measured with SAXS at various polymer concentrations. Numbers give polymer concentrations Φ_P in vol%. The vertical dashed lines mark the ratio $q_0 \div q_1 \div q_2 \div q_3 = 1 \div \sqrt{3} \div 2 \div \sqrt{7}$ for the sample with $\Phi_P = 16.6$ vol%. The insert shows the radial mass distribution obtained for the bottle-brush polymer.

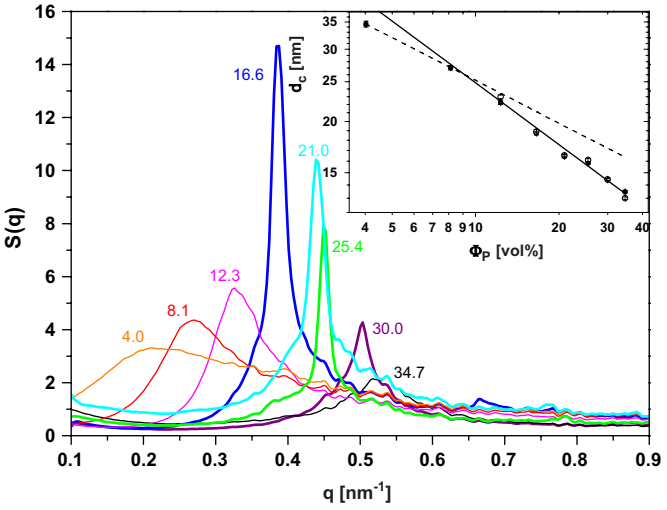

Fig. 9. Structure factors obtained from the measured SAXS spectra as described in the text. Numbers give polymer concentrations Φ_P in vol%. The insert shows the inter-cylinder distances as a function of Φ_P determined from q_0 (filled symbols) and q_1 (empty symbols), respectively. The solid and dashed line show the result of a fit to Eq. (18) with $\beta = 1/2$ and $\beta = 1/3$, respectively.

To allow a comparison of our results to those obtained by Schmidt and coworkers [37] for the lyotropic behavior of a bottle-brush polymers with poly(alkyl methacrylate) backbones and polystyrene side chains we determined the structure factor $S(q)$ from the measured scattering intensities by the application of the equation $S(q) = I(q)/P(q)$. The results are shown in Fig. 9 where for $P(q)$ the experimentally determined form factor was taken. However, caution is advised since (1) $P(q)$ should change with the polymer concentration and (2) the relation only holds if the center-of-mass coordinate and the vectors pointing to the individual scattering units inside a particle are not correlated which is not true for aligned, asymmetric particles.

With increasing polymer concentrations the first peak constantly shifts towards larger q. Schmidt and coworkers [37] found an increasing peak intensity at fixed peak position for lower polymer contents ($\Phi_P < 12$ vol%) and interpreted their results as indication for a biphasic region in which, they argue, the amount of the anisotropic phase increases at fixed interparticle spacing. For higher polymer concentrations they also deduced the appearance of a hexagonal phase from the location of higher order peaks. In the insert in Fig. 9 the distance between adjacent cylinders d_c determined from $S(q)$ by means of Eq. (17) is shown. In addition we determined d_c from I(q) from the q_1 position which should be less affected by concentrational changes of the form factor. There is good agreement between the values determined by the different methods. The lines in the insert of Fig. 9 show the scaling behavior

$$d_c \approx d_0 \Phi_P^{-\beta} \tag{18}$$

where d_0 is the hard-core diameter of the bottle-brush. For packing of parallel cylinders $\beta = 1/2$ and for the isotropic case $\beta = 1/3$ is expected. Despite the deviation for the lowest concentration measured, scaling with $\beta = 1/2$ is well preserved.

The hard-core diameter $d_0 = 7.84 \pm 0.09$ nm is, as expected, smaller than twice the cross section radius of gyration $2 \times R_{CS,g} = 10.2 \pm 0.2$ nm. However, it is larger than the hypothetical hard-core diameter $d_{hc} \approx 5.9$ nm calculated from the overall molecular weight and contour length of the brush using the bulk density of p*n*BA of $\rho = 1.087$ g/cm^3. Up to a polymer concentration of about 12.3 vol% no higher order peaks appear. Thus, most likely the system is in the isotropic phase and the first order peak is only a measure of the mean inter-cylinder spacing. At a volume fraction of 16.6 vol% the sharp and intense first order peak as well as the higher order peaks indicate a hexagonal ordering. However, going to even higher concentrations there are clearly broader peaks underneath the sharper Bragg peaks indicating a coexistence of an isotropic and a hexagonal phase. At the highest concentration the higher order peaks have disappeared and only a broad first order peak is left indicating again a solely isotropic phase. Most likely the melting of the ordered structure is due to the fact that at a concentration of about 21.0 vol% the bottle-brush polymers significantly interpenetrate each other. As can be seen from a comparison of the inserts included in Figs. 8 and 9 at $\Phi_P = 21.0$ vol% the inter-particle spacing is significantly smaller than the radial extension of the bottle-brush polymer. The radial mass distribution $\rho_{CS}(r) \times r^2$ shown in Fig. 9 was calculated using Eq. (8) with σ_C obtained from a model fit of the scattering spectra as described in Section 2.2. However, excluded volume interaction which is the driving force for the ordering is increasingly screened as soon as the brushes start to interpenetrate each other.

4. Conclusions

We investigated the structure of bottle-brush polymers by means of scattering experiments and computer simulations. Good qualitative agreement between the measured form factors and those calculated from the simulated structures was obtained. Both the simulation as well as the experimental results indicate a side chain conformation close to that of an unperturbed 3D-SAW. The backbone adopts a stretched conformation in the brush. The extent of stretching and the increase in the persistence length of the backbone increases with side chain and backbone length. However, saturation is reached at about $N_s \approx N_b/2$. Thus, increasing the side chain length does not lead to more persistent overall structures. The ratio l_p/d, determining whether lyotropic behavior can be expected, decreases with N_s for longer side chains. However, there are also limitations in decreasing d since for very short side chains l_p starts to decrease. Even though l_p/d is rather small for our samples (experimental value ≈ 4) we observe lyotropic behavior. At low polymer concentrations the bottle-brush polymer solution is isotropic. With increasing Φ_P the data indicate the appearance of a hexagonal phase. Increasing the concentration further, the hexagonal phase seems to coexist with an isotropic phase and, finally, the ordered phase disappears at the highest concentration due to screening of the excluded volume interactions when the bottle-brush polymers significantly interpenetrate each other.

Acknowledgements

We appreciate Dr. Burkhard Dünweg for the fruitful discussions.

References

[1] Zhang MF, Mueller AHE. J Polym Sci, Part A 2005;43:3461–81.
[2] Rathgeber S, Pakula T, Wilk A, Matyjaszewski K, Beers KL. J Chem Phys 2005;122:124904.
[3] Wataoka I, Urakawa H, Kajiwara K, Schmidt M, Wintermantel M. Polym Int 1997;44:365–70.
[4] Fischer K, Schmidt M. Macromol Rapid Commun 2001;22:787–91.
[5] Terao K, Nakamura Y, Norisuye T. Macromolecules 1999;32:711–6.
[6] Hokajo T, Terao K, Nakamura Y, Norisuye T. Polym J 2001;33:481–5.
[7] Wintermantel M, Gerle M, Fischer K, Schmidt M, Wataoka I, Urakawa H, et al. Macromolecules 1996;29:978–83.
[8] Gerle M, Fischer K, Roos S, Müller AHE, Schmidt M, Sheiko SS, et al. Macromolecules 1999;32:2629–37.
[9] Nemoto N, Nagai M, Koike A, Okada S. Macromolecules 1995;28:3854–9.
[10] Murat M, Grest GS. Macromolecules 1991;24:704–8.
[11] Gauger A, Pakula T. Macromolecules 1995;28:190–6.
[12] Rouault Y, Borisov OV. Macromolecules 1996;29:2605–11.
[13] Saariaho M, Ikkala O, Szleifer I, Erukhimovich I, ten Brinke G. J Chem Phys 1997;107:3267–76.
[14] Saariaho M, Szleifer I, Ikkala O, ten Brinke G. Macromol Theory Simul 1998;7:211–6.
[15] Saariaho M, Subbotin A, Szleifer I, Ikkala O, ten Brinke G. Macromolecules 1999;32:4439–43.
[16] Saariaho M, Subbotin A, Ikkala O, ten Brinke G. Macromol Rapid Commun 2000;21:110–5.
[17] Shiokawa K, Itoh K, Nemoto N. J Chem Phys 1999;111:8165–73.
[18] Khalatur PG, Shirvanyanz DG, Starovoitova NY, Khokhlov AR. Macromol Theory Simul 2000;9:141–55.
[19] Halperin A, Tirrell M, Lodge TP. Adv Polym Sci 1992;100:31–71.
[20] Fredrickson GH. Macromolecules 1993;26:2825–31.
[21] Birshtein TM, Borisov OV, Zhulina YB, Khokhlov AR, Yurasova TA. Polym Sci, USSR 1987;29:1293–300.
[22] Subbotin A, Saariaho M, Ikkala O, ten Brinke G. Macromolecules 2000; 33:3447–52.
[23] Nakamura Y, Norisuye T. Polym J 2001;33:874–8.
[24] van der Schoot P. J Chem Phys 1996;104:1130–9.
[25] Wang JS, Matyjaszewski K. J Am Chem Soc 1995;117:5614–5.
[26] Matyjaszewski K, Xia J. Chem Rev 2001;101:2921–90.
[27] Börner H, Matyjaszewski K. Macromol Symp 2002;177:1–15.
[28] Beers K, Gaynor S, Matyjaszewski K, Sheiko SS, Möller M. Macromolecules 1998;31:9413–5.
[29] Börner HG, Duran D, Matyjaszewski K, da Silva M, Sheiko SS. Macromolecules 2002;35:3387–94.
[30] Matyjaszewski K, Ziegler MJ, Arehart SV, Greszta D, Pakula T. J Phys Org Chem 2000;13:775–86.
[31] Pedersen JS, Posselt D, Mortensen K. J Appl Crystallogr 1990;23:321–33.
[32] Pedersen JS, Schurtenberger P. Macromolecules 1996;29:7602–12.
[33] Dozier WD, Huang JS, Fetters LJ. Macromolecules 1991;24:2810–4.
[34] Pakula T. Simulation on the completely occupied lattice. In: Kotelyanskii MJ, Theodorou DN, editors. Simulation methods for polymers. NewYork: Dekker; 2004 [chapter 5].
[35] Pakula T, Jeszka K. Macromolecules 1999;32:6821–30.
[36] Neugebauer D, Zhang Y, Pakula T, Sheiko SS, Matyjaszewski K. Macromolecules 2003;36:6746–55.
[37] Wintermantel M, Fischer K, Gerle M, Ries R, Schmidt M, Kajiwara K, et al. Angew Chem Int Ed 1995;34:1472–4.